BIOCHEMISTRY
including biophysical chemistry & molecular biology

Article

pubs.acs.org/biochemistry

Gelsolin-like Activation of Villin: Calcium Sensitivity of the Long Helix in Domain 6

Stanislav O. Fedechkin,[†] Jacob Brockerman,[†] Danielle A. Pfaff,[†] Lucian Burns,[†] Terry Webb,[†] Alexander Nelson,[†] Fengli Zhang,[‡] Anton V. Sabantsev,[§] Alexey S. Melnikov,[§] C. James McKnight,[∥] and Serge L. Smirnov*[,†]

[†]Department of Chemistry, Western Washington University, 516 High Street, Bellingham, Washington 98225-9150, United States

[‡]National High Magnetic Field Laboratory, Florida State University, 1800 East Paul Dirac Drive, Tallahassee, Florida 32310-3706, United States

[§]Institute for Nanobiotechnologies, Saint Petersburg State Polytechnical University, Polytechnicheskaya 29, 197376 St. Petersburg, Russia

[∥]Department of Physiology and Biophysics, Boston University School of Medicine, 700 Albany Street, Boston, Massachusetts 02118-2526, United States

Supporting Information

ABSTRACT: Villin is a gelsolin-like cytoskeleton regulator localized in the brush border at the apical end of epithelial cells. Villin regulates microvilli by bundling F-actin at low calcium levels and severing it at high calcium levels. The villin polypeptide consists of six gelsolin-like repeats (V1−V6) and the unique, actin binding C-terminal headpiece domain (HP). Villin modular fragment V6-HP requires calcium to stay monomeric and bundle F-actin. Our data show that isolated V6 is monomeric and does not bind F-actin at any level of calcium. We propose that the 40-residue unfolded V6-to-HP linker can be a key regulatory element in villin's functions such as its interactions with F-actin. Here we report a calcium-bound solution nuclear magnetic resonance (NMR) structure of V6, which has a gelsolin-like fold with the long α-helix in the extended conformation. Intrinsic tryptophan fluorescence quenching reveals two-K_d calcium binding in V6 (K_{d1} of 22 μM and K_{d2} of 2.8 mM). According to our NMR data, the conformation of V6 responds the most to micromolar calcium. We show that the long α-helix and the adjacent residues form the calcium-sensitive elements in V6. These observations are consistent with the calcium activation of F-actin severing by villin analogous to the gelsolin helix-straightening mechanism.

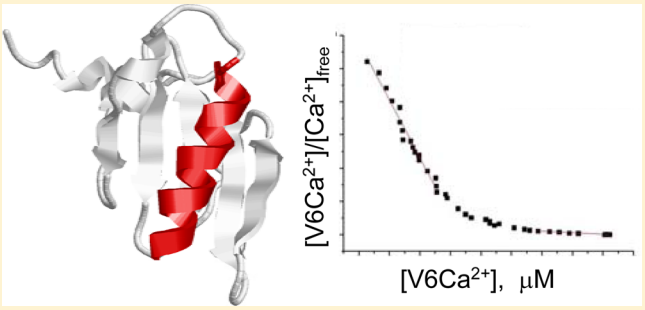

Villin is an 826-residue, modular protein found in the brush border of the absorptive epithelial cells in the gut and kidney and is implicated in the upkeep of microvilli.[1] Villin is a member of the gelsolin superfamily of actin-regulating proteins.[2] Representative proteins from this family include severin,[3] gelsolin,[2] supervillin,[4] and archvillin.[5,6] The amino acid sequence of villin includes two distinct parts: the large, N-terminal, gelsolin-like core and the compact C-terminal "headpiece" domain connected to the core via an unstructured, 40-residue linker[2,7] (Figure 1). The sequence of the villin core is ∼50% identical with that of gelsolin and includes six homologous repeats (V1−V6)[2] (Figure 1A,B), with repeat V6 connected to the headpiece via the linker. Each repeat consists of ∼100−120 residues and forms a common structural motif: a five-stranded β-sheet sandwiched between one long α-helix and two short α-helices connected by loops[8,9] (Figure 1B).

Villin is regulated by several factors, including calcium levels,[2] tyrosine phosphorylation,[1] and phosphatidylinositol 4,5-bisphosphate (PIP2).[10] Villin can bundle actin filaments (F-actin) at physiological calcium levels and sever, cap, and nucleate the filaments in response to rising calcium levels,[2] phosphorylation,[11] or other factors.[10] The capacity of villin to bind and bundle F-actin *in vitro* explains its role in the upkeep of the brush border and microvilli of the apical surface of the epithelial cells.[12] At the same time, the ability of villin to sever and cap F-actin at elevated calcium levels may be another principal role of villin in the regulation of microvilli and/or cell turnover.[13]

According to one of the models, villin cross-links F-actin into bundles[2] using one F-actin binding site in the core domain, similar to gelsolin,[12] and the second F-actin binding site on the C-terminal headpiece domain.[12,14,15] An alternative model states that villin can form dimers via its gelsolin-like core and present two headpiece domains to bundle actin filaments.[16]

Received: June 3, 2013
Revised: September 25, 2013
Published: September 26, 2013

   dx.doi.org/10.1021/bi400699s | *Biochemistry* 2013, 52, 7890−7900

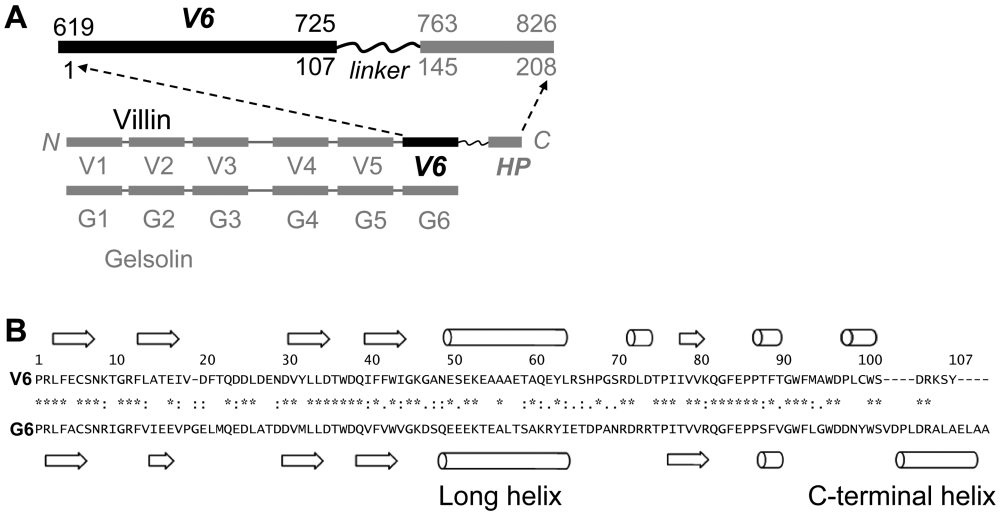

Figure 1. (A) Diagram of the primary structure of V6-HP (top), villin (middle), and gelsolin (bottom). V6 is colored black in the V6-HP (top) and villin (middle) diagrams. The numbers on top of the V6-HP drawing correspond to the positions in the chicken villin sequence.[7] The numbers on the bottom define these positions in the V6 and V6-HP constructs and are used by default throughout this work. (B) Sequence alignment (ClustalW[58]) and secondary structure of chicken V6 (for our data, see Figure 4) and mouse G6.[8,9] Cylinders denote α-helices and arrows β-strand elements. ClustalW alignment legend: asterisk, identical match; colon, strongly similar; period, weakly similar.[58] Every 10th position in V6 is marked with the residue number above the sequence.

However, electron tomography imaging demonstrates that monomeric villin cross-links F-actin filaments.[17] The chimeric protein containing the villin headpiece attached to gelsolin cannot bundle F-actin,[14] highlighting the crucial role of the villin core.

Like gelsolin, villin can also sever actin filaments in a Ca^{2+}-dependent manner. The actin-severing function of villin requires a significantly higher level of Ca^{2+} than gelsolin. At basal (submicromolar) levels of Ca^{2+}, gelsolin is inactive. The protein switches into the F-actin severing mode at an elevated Ca^{2+} concentration (~10 μM).[18] Villin, on the other hand, requires 100−200 μM Ca^{2+} for *in vitro* activation of its actin-severing capacity,[19] a level accessible in the cell only during the state of apoptosis. However, phosphorylation of the villin core, including the V6 domain,[1,11] allows actin severing by villin at nanomolar Ca^{2+} concentrations.

The Ca^{2+} activation of the actin-severing function of gelsolin is done via the "latch and hinge" mechanism.[18] At low Ca^{2+} levels, the long helix of G6 adopts an unusual, kinked shape.[8,9] At the same time, the C-terminal "latch" helix autoinhibits gelsolin by interacting and binding with domain 2 (G2) stabilizing a closed, inactive conformation.[8,9] This sterically occludes the G2−actin binding site.[20] With an increase in the Ca^{2+} level, the C-terminal latch helix detaches from the G2 domain, and the "hinge" opens. The N- and C-terminal halves of gelsolin (G1−G2−G3 and G4−G5−G6, respectively) disengage. In the open conformation, the long helix of G6 becomes straight. One of the most fundamental questions regarding villin is whether it has a similar, calcium-dependent open and closed conformation mechanism for activation. Villin undergoes a large calcium-induced (threshold of ≈20 μM Ca^{2+}) conformational change suggesting open and closed conformations.[21] The properties of villin domain 6 (V6) (Figure 1) need to be clarified to understand its role in the control of villin function.

Previously, we have examined the V6-HP region of chicken villin, which contains the V6 and headpiece (HP) domains connected by a linker sequence.[7] This modular fragment is monomeric and, surprisingly, bundles F-actin, making it a remarkably small actin-bundling protein system. In the absence of Ca^{2+}, V6-HP aggregates and is unable to bundle F-actin. At high Ca^{2+} concentrations, V6-HP is soluble, with the V6 and HP fragments forming distinct domains tethered by a 40-residue flexible and disordered linker sequence. The particular role of this linker is unknown. The headpiece in V6-HP adopts the same fold as in isolation.[7] Therefore, one of the actin binding sites within V6-HP is associated with the headpiece domain, which leaves V6 and/or the linker as the location of the other actin binding site. The villin headpiece is insensitive to calcium and does not require Ca^{2+} for its structure or for F-actin binding.[14,22,23] Thus, the calcium binding sites of V6-HP were proposed to be located on V6 and/or the linker.

Recently, an attempt to crystallize the human villin V4−V5−V6 three-domain fragment in complex with G-actin in the absence of Ca^{2+} was reported.[24] Surprisingly, the resulting map showed electron density for the V6 domain only. Electron density from actin and the V4 and V5 domains was absent.[24] In that crystal structure, V6 forms a two-domain asymmetric unit (dimer) showing a typical gelsolin-like fold with the long helix in the extended (straight) conformation [Protein Data Bank (PDB) entry 3FG7]. This calcium-free V6 structure[24] is very similar to the fold of calcium-bound domain 6 of gelsolin (G6),[8,25] with the long helix being straight in both domains. In contrast, the calcium-free G6 domain (in the context of the G4−G5−G6 fragment) has its long helix kinked.[9] The crystal structure of calcium-free villin V6 suggests that calcium regulation of its long helix may differ from that of the gelsolin G6 domain. Alternatively, V6 could be in the active, severing conformation in the calcium-free crystal structure,[24] because of the particular context (e.g., isolated V6 vs V4−V5−V6 fragment).

We would like to know whether V6 has its long helix in an extended (straight) conformation in a high-calcium environment and whether the helix undergoes a change in shape with decreased calcium levels. We also would like to compare the structure of the isolated V6 with that of V6-HP (and G6) and

dx.doi.org/10.1021/bi400699s | *Biochemistry* 2013, 52, 7890−7900

determine the affinity of V6 for calcium and its capacity to dimerize and bind F-actin.

We find that with or without calcium, the isolated V6 domain remains monomeric and is unable to bind F-actin in contrast to V6-HP. We probed the affinity of V6 for calcium with tryptophan fluorescence and determined that the domain displays two-K_d calcium binding (K_{d1} of 22 μM and K_{d2} of 2.8 mM). The conformation of V6 is most sensitive to the micromolar calcium level. We report the solution NMR structure of chicken villin domain V6 in the calcium-bound form (5 mM Ca^{2+}). The domain adopts a gelsolin-like fold with the long helix extended (straight), consistent with the one observed in the calcium-bound crystal structure of the gelsolin G6 domain.[8,25] We propose that villin and gelsolin share a similar mechanism of calcium-induced F-actin severing activity via the straightening of the long α-helix in V6 and G6.

MATERIALS AND METHODS

Construction of the pV6 Expression Vector. The expression vector (pV6) was designed on the basis of the pF6-HP vector described previously,[7] with the TGA stop codon introduced after Tyr107 via the QuikChange site-directed mutagenesis kit (Agilent Technologies, Inc., Santa Clara, CA) according to the supplied protocol.

^{15}N- and ^{13}C/^{15}N-Labeled V6 Sample Preparation. The V6 villin fragment was overexpressed from the pV6 plasmid in *Escherichia coli* BL21-(DE3) (Novagen) using the protocol described by Marley et al.[26] Briefly, cells were grown at 37 °C in Luria broth to an OD_{600} of ~0.6, at which point they were induced with IPTG (0.8 mM) and grown for additional 4 h. After that, they were harvested by centrifugation at 3000*g* for 30 min. To express protein samples labeled with ^{15}N and ^{13}C isotopes, the cells were grown to an OD_{600} of ~0.6 and transferred from LB to M9T medium by centrifugation at 3000*g* for 30 min, washed in 1 L of the M9T salts, reharvested, and transferred to one-quarter the original culture volume of ^{13}C-/^{15}N-labeled M9T medium for expression.[26] The cells were allowed to equilibrate in the ^{13}C-/^{15}N-labeled M9T medium for 1 h, induced with 0.8 mM IPTG, and harvested after 4 h by centrifugation at ~3000*g* for 30 min. The following lysis and gel filtration steps were performed in buffer A [150 mM NaCl, 5 mM $CaCl_2$, 5 mM dithiothreitol (DTT), 0.01% NaN_3, and 20 mM PIPES buffer (pH 7.0)]. The cells were lysed in buffer A by sonication in the presence of DNase I (1 μg/mL), DTT (50 mM), and lysozyme (50 μg/mL). Cell debris was removed by centrifugation at 40000*g* for 40 min. The filtered supernatant was applied to a Sephadex G50 gravity column (2 cm × 100 cm) run in buffer A at a flow rate of 0.5−1.5 mL/min, and the 3−5 mL fractions were collected and analyzed via sodium dodecyl sulfate−polyacrylamide gel electrophoresis (SDS−PAGE). The fractions containing V6 SDS−PAGE bands of the highest relative purity were combined and concentrated using 15 mL Amicon Ultra Centrifugal units with an Ultracel membrane [molecular weight cutoff (MWCO) of 3000] made by Millipore. These combined and concentrated samples were injected onto the GE Superdex 75 HP-SEC column equilibrated in buffer A. The elution from the FPLC column was monitored by UV absorbance at 280 nm; the V6-containing peak was collected, and its >95% purity was confirmed with SDS−PAGE (Figure S1 of the Supporting Information). Finally, the sample was concentrated and PIPES buffer replaced with d_{18}-PIPES using a 3 kDa MWCO Amicon Ultra-4 spin concentrator (Millipore). DTT was present in all buffers to prevent the formation of disulfides between Cys6 and Cys100, which are expected to remain as free thiols in the reducing environment inside the cell. Protein concentrations were determined by UV absorbance at 280 nm.[27] The expression of the unlabeled V6 samples was performed similarly with Luria broth utilized throughout the procedure.

Size-Exclusion Chromatography of V6. Size-exclusion (FPLC) chromatograms of V6 (12.4 kDa) were recorded in PIPES buffer [20 mM PIPES (pH 7.0), 150 mM NaCl, 0.01% NaN_3, and 5 mM DTT] with and without calcium at room temperature. V6 was run in a Superdex 75 10/300 column (GE Healthcare) at a flow rate of 0.5 mL/min at room temperature. The concentration of the V6 sample in 5 mM Ca^{2+} was ~50 μM, and the calcium-free V6 concentration was ~400 μM. The chromatograms were rescaled to approximately equal intensity of the V6 peaks.

NMR Data Collection and Processing. The NMR samples consisted of 0.5−1.0 mM ^{13}C-/^{15}N-labeled or unlabeled V6 in 10% ^2H_2O, 5 mM $CaCl_2$, 10 mM d_{10}-DTT, 0.01% NaN_3, and 20 mM d_{18}-PIPES (pH 7.0). No correction for the effect of ^2H_2O was made during the pH adjustment. Two-dimensional (2D) and three-dimensional (3D) NMR data were collected at 25 °C on a Varian INOVA 720 MHz spectrometer with a triple-resonance probe located at the National High Magnetic Field Laboratory facility, and a local 500 MHz Varian INOVA spectrometer with a triple-resonance probe (Western Washington University). The acquired NMR data were processed utilizing NMRPipe.[28]

NMR Resonance Assignment. The backbone resonance (^{1}H, ^{15}N, and ^{13}C) assignment of the V6 sample was performed through a combined use of 2D ^{15}N HSQC[29,30] and the following 3D NMR data sets utilizing the online PINE server[39] followed by a manual check and necessary corrections: HNCACB,[31,32] CBCA(CO)NH,[33] HNCO,[34] HN(CA)CO,[35] HNHA,[36] HNHB,[37] and HBHA(CO)NH.[38] The side chain resonance (aliphatic ^{1}H and ^{13}C) assignments were produced from HCCH-COSY,[40] HCCH-TOCSY,[41] CC(CO)NH,[42] and HC(CO)NH[42] NMR data. Aromatic side chain ^{1}H assignments were derived from aromatic ^{13}C HSQC spectra[30] as well as phase-sensitive[43] ^{1}H 2D NOESY and TOCSY data recorded in 100% ^2H_2O. The visualization and analysis of the NMR spectra and the cross-peak picking were performed with NMRVIEW.[44] Chemical shifts for all the nuclei were referenced relatively to the internal standard 3-(trimethylsilyl)tetradeuterosodium propionate.[45]

Solution NMR Structure Determination of V6. The solution structure of V6 was determined using CYANA 2.1[46] based on the distance and dihedral angle restraints. The distance restraints were derived from the heteronuclear 3D and proton 2D NOESY data recorded in 90% H_2O and assigned automatically during the iterative CYANA simulations, which also concurrently determined the solution structure for the current iteration. The dihedral angle restraints were produced prior to the CYANA simulations with PREDITOR[47] utilizing the backbone chemical shift values of ^{1}H, ^{15}N, $^{13}C_\alpha$, ^{13}CO, and $^{13}C_\beta$. Initially, CYANA simulations utilized only the 3D NOESY sets (^{15}N NOESY, ^{13}C NOESY aliphatic, and ^{13}C NOESY aromatic). Each simulation was conducted according to a standard CYANA protocol (*noeassign* macro) of iteratively determining the solution structure while concurrently assigning the maximally high number of NOE cross-peaks. The simulations started with 600 test conformers and employed 6000 or 10000 steps of torsion angle dynamic steps. The 10

dx.doi.org/10.1021/bi400699s | *Biochemistry* 2013, 52, 7890−7900

conformers with the lowest target function (penalty) were retained for analysis and passed onto the next cycle as well and reported at the end as the lowest-energy ensemble at the end of a particular run. Every simulation was performed with more than one seed value, and the common assignments from the simulations were used as an assigned set of NOEs for the next simulations. The assigned NOESY cross-peaks that resulted in distance restraints violated by more than 0.5 Å at the end of a run were manually converted back to the unassigned status and used as such in the beginning of the next simulation. This process was repeated until no new NOE peaks could be assigned. Once the majority (~90%) of 3D NOESY peaks had been assigned in this way, the 2D ^{1}H NOESY peak set was added and assigned by the same iterative process during CYANA runs while all the previously obtained 3D NOE assignments were kept. At this stage, every assigned 2D or 3D NOE peak generating distance restraint violated by >0.5 Å at the end of a run was manually unassigned for the next simulation. The final structure had a total of 1076 upper distance restraints and a backbone root-mean-square deviation (rmsd) of <0.6 Å for the 10 best structures. Structure 1 in the reported PDB file is suggested as the most representative of the ensemble.

To clarify the secondary structure of the C-terminus, we performed the entire structure determination procedure with the dihedral angle restraints for residues 99−107 removed. The corresponding part of the polypeptide (98−102) retained its helicity, stabilized by the short-range distance restraints, showing that the C-terminal helix is not an artifact of the structure determination calculations.

The obtained structures were visually inspected by Rasmol[48] and the UCSF Chimera package.[49] The final structural ensembles were analyzed with the PSVS online server[50] as required by the PDB for acceptable structure submission.

Calcium Titration of V6 Monitored by NMR. The V6 sample was in 5 mM calcium at the beginning of the EDTA titration. EDTA was then added to decrease the calcium level to 1, 0.5, and 0 mM. Calcium restoration was performed by buffer exchange into 5 mM calcium using a spin concentrator. The resulting HSQC spectrum of the 5 mM V6 sample matched the initial spectrum of V6 with 5 mM calcium. Likewise, the ^{15}N HSQC spectra of V6 recorded at 0 mM calcium and in an excess of EDTA are identical. The number of peaks remained approximately the same at around 150 (using nmrview autopick by setting a minimum threshold) for the ^{15}N HSQC spectra of V6 with 5, 1, 0.5, and 0 mM calcium.

Calcium Titration of V6 Monitored by Tryptophan Fluorescence Quenching. A calcium-free V6 sample [20 mM PIPES (pH 7.0) and 5 mM DTT] was obtained by the initial removal of calcium from solution by buffer exchange (Millipore membrane concentrators, 3000 kDa MWCO), followed by addition of a 100-fold excess of EDTA. Subsequently, EDTA was eliminated by another round of buffer exchange.

The tryptophan fluorescence was recorded with a Cary Eclipse (Varian) fluorometer, with 280 nm excitation (1.5 nm slit) and 350 nm emission (20 nm slit). Samples were kept in a UV−vis grade acrylic cuvette while being magnetically stirred throughout the procedure.

The concentration of V6 was 2.23 μM, and the calcium concentration was changed by addition of appropriate calcium stock solutions. After each addition, the sample was allowed to equilibrate for 2 min before the data were acquired. Our kinetic data suggest that equilibration from 0 to 5 mM Ca^{2+} or vice versa takes <20 s; therefore, equilibration for 2 min for each step is sufficient. At each calcium addition, 100 measurements at 350 nm with an exposure time of 0.2 s were taken and averaged. The emission was monitored throughout the experiment by acquiring fluorescence emission spectra (300−500 nm) via 280 nm excitation. Potential photobleaching was assessed and shown not to cause any detectable changes in fluorescence intensity during the experiment. No significant change in the signal (<0.1%) was observed after continuous exposure for 30 min, which is longer than the duration of the actual experiments.

The fluorescence intensity at 350 nm as a function of calcium concentration was analyzed according to the general methodology describing a reversible protein−ligand (1:1) interaction with K_d as a measure of affinity as previously described.[51,52] The concentrations of calcium and V6 at each step were corrected for the volume of added calcium stocks. Fitting the data to a single-K_d calcium binding model resulted in a poor fit. Fits to a model with two K_d values gave a much improved goodness of fit to the experimental data (Figure S2 and S3 of the Supporting Information).[52] The addition of the second K_d lowered the χ^2 metric ~30 times, which indicates the significant increase in the quality of fit beyond what would be expected simply from additional parameters in the model.

F-Actin Binding by V6. Actin was purchased from Cytoskeleton Inc. (Denver, CO) as a lyophilized powder with a sample purity of >99%. Actin samples were prepared by resuspending actin powder in nanopure H_2O to a final G-actin concentration of 24.0 μM, in 5.0 mM Tris-HCl (pH 7.5), 0.1 mM $CaCl_2$, 0.20 mM adenosine triphosphate (ATP), and 0.50 mM DTT for 1 h at 4 °C. The sample was then spun down at 16000*g* on a benchtop centrifuge for 15 min at 4 °C. The top 90−95% of the supernatant volume was transferred to a new container. G-Actin sample aliquots of 60 μL were transferred to ultracentrifuge tubes, and 6.0 μL of 10× buffer F (500.0 mM KCl, 20.0 mM $MgCl_2$, and 10.0 mM ATP) was added for actin polymerization. Samples were polymerized for 1 h at room temperature. The solution was brought to 120 μL using the same buffer mixture with a final G-actin concentration of 12.0 μM, 4.1 mM Tris-HCl, 1.1 mM ATP, 45 mM KCl, 1.8 mM $MgCl_2$, and 0.4 mM DTT and incubated with either V6 or the villin headpiece (HP67, the last 67 residues of chicken villin[15]) protein fragments. V6 and HP67 protein concentrations of 0, 5, 10, 25, 50, 100, and 200 μM were tested. Calcium concentrations of 0.1 and 5 mM were tested. After being incubated at 4 °C or room temperature for 1 h, samples were spun down for 1 h at 150000*g* in a Sorvall MX-150 ultramicrocentrifuge. The supernatant was removed and the pellet washed with buffer F, and the pellets were resuspended in 7% acetic acid and stored (4 °C or on the bench) for further analysis.

The F-actin/V6 and F-actin/HP67 pull-down samples were analyzed using reverse phase high-performance liquid chromatography (HPLC). A linear gradient from 20 to 80% acetonitrile was run at a flow rate of 1 mL/min through a Beckman Ultrasphere Analytical (C18) column over 1 h. The ion pairing agent used was trifluoroacetic acid (0.1%), and the eluting protein was monitored using UV−vis spectroscopy (λ = 222 nm). Calibration curves were constructed for HP67 and V6 villin fragments using protein samples of standardized concentrations.

RESULTS

The Isolated V6 Domain Exists as a Monomer with and without Calcium. We performed the size-exclusion chromatography study of the V6 sample at 5 mM calcium and in the absence of calcium (Figure 2) to check the V6 oligomeric

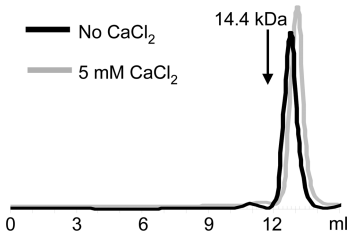

Figure 2. Size-exclusion (FPLC) chromatography of V6 (12.4 kDa) with and without calcium recorded in PIPES buffer (pH 7.0) at room temperature. Elution volumes are 13.1 mL for V6 in 5 mM $CaCl_2$ (light gray) and 12.8 mL for V6 in a calcium-free buffer (black). The arrow marks the elution volume of a molecular mass standard (hen egg white lysozyme, *c*-type, 14.4 kDa, elution volume of 11.8 mL) run separately; 250 μL of V6 was run in a Superdex 75 10/300 column (GE Healthcare) in gel filtration buffer [20 mM PIPES, 150 mM NaCl, and 5 mM DTT (pH 7.0)] at a flow rate of 0.5 mL/min at room temperature. The concentration of the V6 sample in 5 mM Ca^{2+} was ~50 μM, and that of calcium-free V6 was ~400 μM. The chromatograms were rescaled to approximately equal intensity of the V6 peaks.

state. With or without calcium, V6 showed single-peak elution chromatograms (Figure 2). The elution volumes for V6 (12.4 kDa) at 5 mM calcium and in a calcium-free buffer were 13.1 and 12.8 mL, respectively. This difference indicates a slightly larger effective radius of gyration of the calcium-free sample, possibly reflecting conformational differences between the two samples. Both V6 samples have elution volumes greater than that of calcium-independent hen egg white lysozyme, *c*-type (14.4 kDa),[53] demonstrating that V6 is monomeric in both high-calcium and calcium-free environments.

The Isolated V6 Domain Adopts a Typical Gelsolin-like Fold at High Calcium Concentrations. The ^{15}N HSQC spectrum of the V6 domain of villin recorded in 5 mM Ca^{2+} contains the expected number of well-dispersed cross-peaks indicating a single, folded conformation (Figure 3). The solution NMR structure of the isolated V6 domain was determined on the basis of distance restraints from 2D and 3D NOESY spectra and chemical shift-based dihedral angle restraint data utilizing the CYANA algorithm.[46] Table 1 lists the statistics for the ensemble of the 10 best final structures (backbone rmsd of ≤1.0 Å for heavy atoms of residues 8−99). The overall fold of V6 is typical for gelsolin-like domains: a central core of five β-strands sandwiched between the long α-helix on one side and loops with a shorter helix on the other (Figure 4A,B). Our solution structure of V6 at a high calcium concentration has a high degree of structural homology with the calcium-free crystal structure of the V6 domain of human villin determined with domains V4 and V5 and actin present but not observed.[24] An rmsd value of ~1.5 Å for 64 backbone C_α atoms forming the core of the domains was reported by the MatchMaker facility of Chimera. Markedly, the long helix in both structures adopts the extended (straight) conformation. Certain local differences between this high-calcium solution V6 structure and published calcium-free V6 crystal structure exist

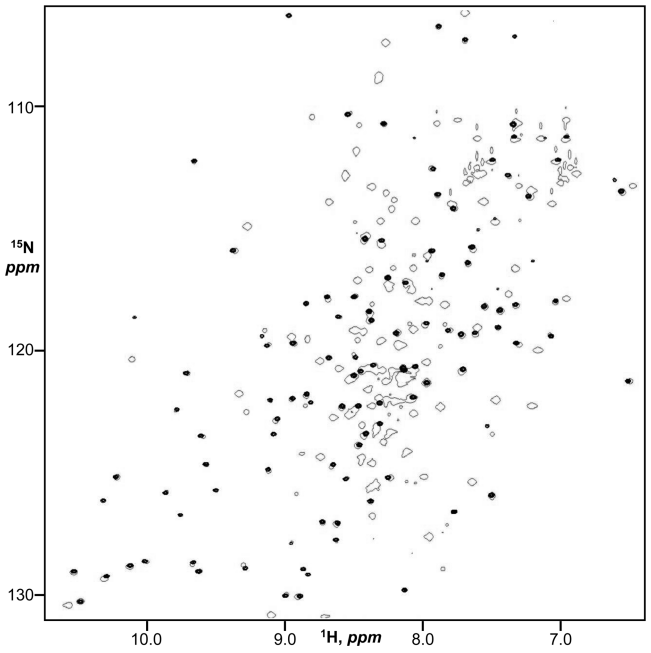

Figure 3. ^{15}N HSQC spectrum of 1 mM V6 (black, multiple levels, recorded at a field strength of 720 MHz) and 1.1 mM V6-HP (gray, single level, recorded at a field strength of 800 MHz). Both spectra were recorded at 25 °C and pH 7.0 in 5 mM Ca^{2+}.

Table 1. Statistics of V6 Structure Calculations

no. of NOE distance constraints	
total	1052
intraresidue ($i = j$)	335
sequential ($\|i - j\| = 1$)	338
medium-range ($1 < \|i - j\| < 5$)	140
long-range ($\|i - j\| \geq 5$)	239
constraints per residue	9.8
no. of long-range constraints per residue	2.2
no. of dihedral angle constraints	402
no. of NOE and dihedral constraints per residue[a]	13.6
no. of distance violations per model[a]	
0.1−0.2 Å	24
0.2−0.4 Å	19
>0.4 Å	0
no. of dihedral angle violations per model[a]	
1−7.2°	45
>7.2°	0
average rmsd from the mean for the 10 best models (Å)	
all backbone atoms (residues 8−99)	0.6
all heavy atoms (residues 8−99)	1.0

[a]Average values.

in the area of the unstructured A−B loop [residues 9−12 (Figure 4C)].

Within the ensemble of the 10 best NMR structures, two regions of the V6 polypeptide are clearly the most disordered elements: residues 65−71 and 104−107 (Figure 4A). Residues 65−71 form the loop following the C-terminus of the long helix (Figure 4A). This loop differs noticeably in conformation from the respective element of calcium-free human V6 (Figure 4C). The other relatively disordered stretch (positions 104−107) forms the C-terminus of the V6 fragment (Figure 4A) that follows a short α-helix (positions 98−102).

dx.doi.org/10.1021/bi400699s | *Biochemistry* 2013, 52, 7890−7900

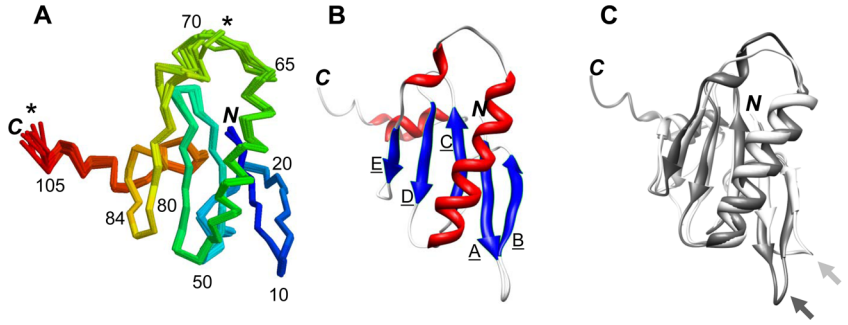

Figure 4. (A) Villin V6 domain, from the 10 best solution NMR structures. The asterisks denote the long loop of residues 64−78 and the C-terminus as the least defined elements of the polypeptide. Selected residue numbers are indicated for reference. The backbone is colored by residue position in the polypeptide chain from blue (N-terminus) through green, yellow, and orange to red (C-terminus). (B) Representative secondary structure of V6. The V6 domain displays a typical gelsolin-like motif with five β-strands (A−E, blue) sandwiched between the long helix (front, red) and short helices (back, red). (C) Calcium-bound chicken villin V6 (gray) aligned with calcium-free human V6 [PDB entry 3FG7 (white)]. Arrows mark the A−B loop showing different conformations in the NMR (dark gray arrow) and crystal (light gray arrow) structures. The gray italicized N and C mark the amino and carboxy termini, respectively.

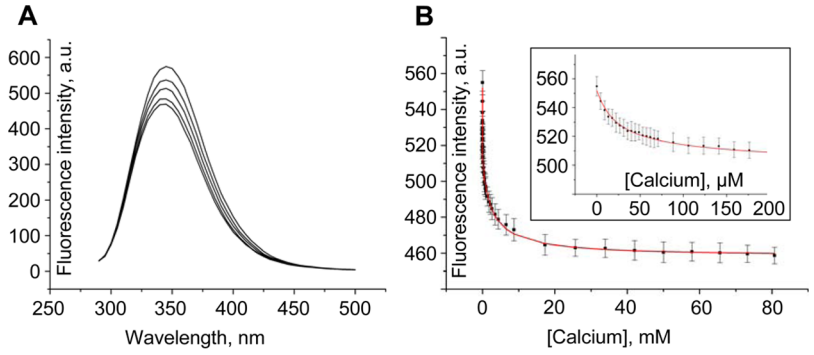

Figure 5. (A) Tryptophan fluorescence emission spectra of V6. Spectra were acquired at five calcium levels: 0 μM, 22 μM, 440 μM, 8.7 mM, and 81 mM. The magnitude of the fluorescence signal decreased as the level of calcium was increased. (B) Full Calcium titration of V6. The fluorescence signal was acquired at 350 nm, which corresponds to the maximum of the spectrum at 0 μM calcium. Each point is the average of 100 individual measurements. The error bars indicate the standard deviation; the actual error is 10 times lower. The insert shows a magnification of the curve at very low calcium concentration.

The V6 Domain Exhibits Two-K_d Binding of Calcium. We measured the affinity of V6 for calcium by the intrinsic tryptophan fluorescence quenching in response to addition of Ca^{2+} to the initially calcium-free V6 sample. The fluorescence spectra showed the maxima near 350 nm with the intensity decreasing as the level of calcium increased (Figure 5A). The calcium-dependent fluorescence signal at 350 nm was recorded in the micromolar to millimolar calcium concentration range (0 μM to 80 mM) (Figure 5B). The data fit well to a model with two independent dissociation constant values: K_{d1} of 22 ± 2 μM and K_{d2} of 2.8 ± 0.2 mM (Figure 5B and Figure S2A−D of the Supporting Information). Scatchard analysis of the data confirms the two-K_d mode of calcium binding by V6 (Figure S2E of the Supporting Information). Fitting the data to the one-K_d curve produced a poor fit (Figure S3 of the Supporting Information). The *F*-test[54] showed that addition of the second K_d to the model was statistically significant ($p < 0.00001$). The fluorescence spectra were reversible with respect to calcium binding as addition of excess EDTA to the 5 mM calcium sample restored the original no-calcium spectrum.

The Calcium Sites on the V6 Domain Localize to the Long Helix and Surrounding Core. We performed a calcium back-titration by addition of EDTA to our NMR sample and monitored chemical shift changes via ^{15}N HSQC NMR spectra (Figure 6). We compared the spectra recorded at 0 and 500 μM calcium (Figure 6A) to assess the conformational changes associated with high-affinity calcium binding (K_d = 22 μM). We also compared the spectra at 1 and 5 mM calcium to characterize the conformational alterations associated with low-affinity (K_d = 2.8 mM) calcium binding (Figure 6B).

The V6 spectra recorded at 0 and 500 μM calcium show major differences indicating substantial conformational change (Figure 6A). For the majority of the residues in calcium-free V6, the ^{15}N HSQC resonances were significantly shifted and could not be unambiguously assigned to their counterparts in the high-calcium V6 spectra (Figures 3 and 6A). For a subset of V6 residues (12, 22, 24, 40, 69, 83, 89−94, 96, 99, 100, 102−104, 106, and 107), the ^{15}N HSQC peaks have similar chemical shifts under high-calcium (5 mM) and calcium-free conditions.

In comparison to Figure 6A, the spectra for V6 recorded at 5 and 1 mM calcium are highly similar, with a majority of the cross-peaks overlapping (Figure 6B). In the spectrum recorded at 1 mM calcium, the cross-peaks for just five residues could not be reliably identified by transferring their assignments from the 5 mM spectrum (residues 45, 52, 62, 71, and 95). Only 20 residues (6, 10, 16, 21, 25, 26, 28, 30−33, 50, 55, 57, 59, 63, 65, 67, 75, and 82) show any noticeable chemical shifts differences (0.045−0.093 ppm for ^{1}H or 0.300−0.816 ppm for ^{15}N).

At High Calcium Concentrations, Isolated V6 Has the Same Fold as in V6-HP. The chemical shift values in isolated V6 are in agreement with the previously published values for

dx.doi.org/10.1021/bi400699s | *Biochemistry* 2013, 52, 7890−7900

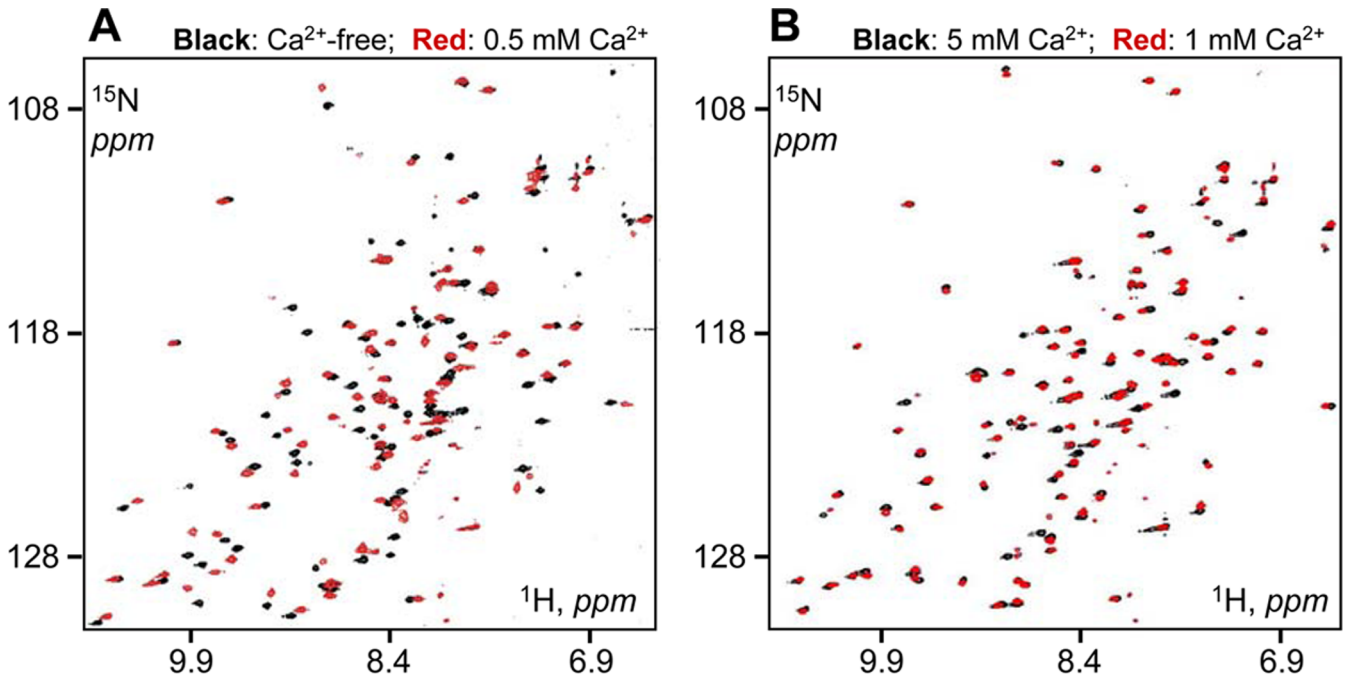

Figure 6. NMR-monitored sensitivity of V6 to micromolar and millimolar calcium levels. (A) Overlay of ^{15}N HSQC spectra of chicken calcium-free V6 (black) and V6 in 0.5 mM Ca^{2+} (red). (B) Overlay of ^{15}N HSQC spectra of V6 in 5 mM Ca^{2+} (black) and 1 mM Ca^{2+} (red). The spectra are referenced and the windows show identical ranges so that a comparison across panels A and B can be made. All spectra were recorded at 25 °C.

V6-HP,[7] with both proteins being in 5 mM calcium (Figure 3 and Figure S4 of the Supporting Information). For all the residues assigned in both V6 and V6-HP (excluding residues 84, 106, and 107), the absolute value of the differences between ^{1}H chemical shifts for the corresponding V6 and V6-HP peaks are <0.045 ppm (Figure S4A of the Supporting Information). The analogous difference in the ^{15}N dimension is <0.35 ppm for all these residues (Figure S4B of the Supporting Information). Such a close match between the resonances of calcium-bound V6 and V6-HP fragments indicates that the V6 domain adopts the same fold in isolation and within the V6-HP context. Residues 105−107 form the V6-to-linker interface in V6-HP, which explains their chemical shift differences between V6 and V6-HP. The large chemical shift difference between V6 and V6-HP samples for residue Phe84 (0.63 ppm for ^{1}H and −6.3 ppm for ^{15}N) may be explained by the proximity of Phe84 to the interface between the folded core and the dynamic, solvent-accessible C-terminus of V6 (Figure 4A). In addition, the NMR spectra of calcium-free V6 in isolation and in V6-HP are similar. A majority of the ^{15}N HSQC cross-peaks in these two samples are closely positioned (Figure S5 of the Supporting Information).

The Isolated V6 Domain Does Not Bind F-Actin. To test the capacity of V6 to bind F-actin, we utilized the F-actin sedimentation assays with the isolated villin headpiece domain (HP67)[23] used as a positive (actin binding) control. The V6 sample showed no detectable affinity for actin filaments with or without calcium (Figure 7). At the same time, the villin headpiece displayed a characteristic saturating hyperbolic binding pattern (Figure 7). We therefore conclude that the V6 domain in isolation does not have a complete, functional F-actin binding site.

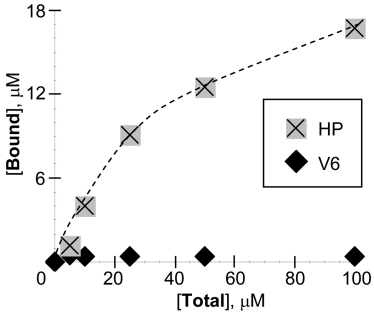

Figure 7. Representative F-actin pull-down assays of V6 (◆) and HP67 (× on a gray background). The *x*-axis shows the concentration of V6 or HP67 samples added to the reaction mixture. The *y*-axis shows the concentration of V6 and HP67 pulled down with F-actin by ultracentrifugation. HP67 points form a distinct hyperbolic curve indicating specific binding to F-actin. V6 has no measurable binding within the range of concentrations tested. Changing the calcium level (5.0 or 0.2 mM) or temperature (25 or 4 °C) did not result in any measurable increase in the level of F-actin binding by V6 (not shown). The standard errors of the mean values were 0.019 μM for V6 (n = 3) and 2.8 μM for HP67 (n = 1).

DISCUSSION

The Long Helix and Adjacent Residues of V6 Show Calcium Sensitivity. One of the goals of our study was to shed light on the mode of interaction of the isolated villin V6 domain with calcium. The capacity of V6 to bind calcium was suggested previously[7] and proposed to play a role in calcium regulation similar to that of the "latch and hinge" mechanism of gelsolin.[51] The exact calcium binding residues in V6 remain undetermined with the N-terminus of its long helix proposed to be the calcium binding area based on homology with G6 (Asn29, Asp30, and Glu52).[7,25]

Here we determined that calcium binding by V6 fits a two-K_d model, with distinct K_d values of 22 μM and 2.8 mM. Our

dx.doi.org/10.1021/bi400699s | Biochemistry 2013, 52, 7890−7900

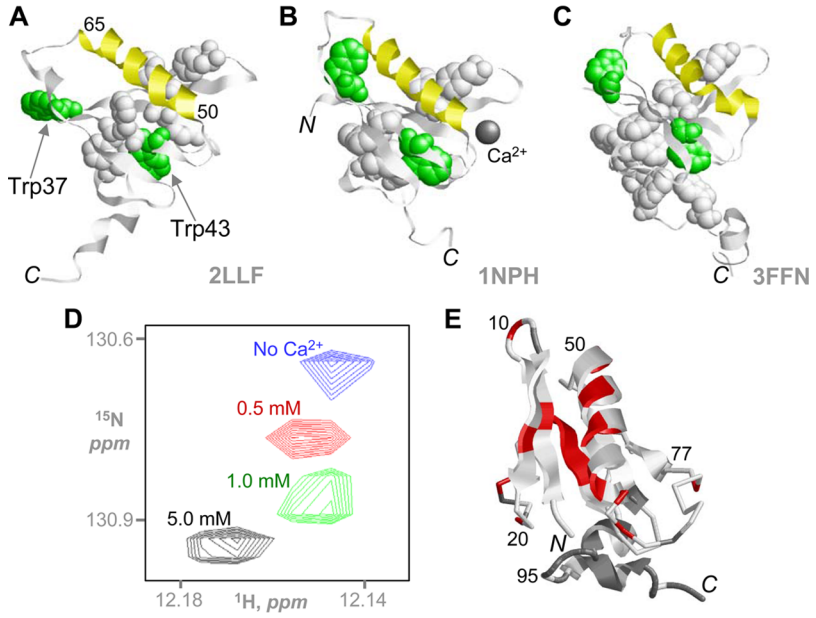

Figure 8. Comparison of V6 and G6 at high and low calcium concentrations. (A) High-calcium structure of V6 from this study (PDB entry 2LLF), showing the location of calcium-sensitive tryptophans (green, Trp43 and Trp37). (B) Calcium-bound structure of G6 (PDB entry 1NPH) showing the bound calcium ion (gray sphere labeled Ca^{2+}). (C) Calcium-free G6 structure (PDB entry 3FFN). Panels B and C have residues corresponding to Trp43 and Trp37 colored green as in panel A. The aromatic regions at or near the long α-helix are shown as white space-filling diagrams. The conformation of the long α-helix (extended in calcium-bound V6 and G6 and kinked in calcium-free G6) is colored yellow in panels A–C. (D) ^{15}N HSQC monitoring of Trp43. The blue, red, green, and black peaks correspond to the Trp43 side chain ($H_{\varepsilon 1}$) in V6 structures with 0, 0.5, 1.0, and 5 mM Ca^{2+}, respectively. (E) Residues in V6 (PDB entry 2LLF), which show significant chemical shift alterations (0.045–0.093 ppm for ^{1}H or 0.300–0.816 ppm for ^{15}N) caused by the change in the calcium level from 5 to 1 mM (Figure 6B), colored red (residues 6, 10, 16, 21, 25, 26, 28, 30–33, 50, 55, 57, 59, 63, 65, 67, 75, and 82). Residues that show no significant chemical shift alterations between 0 and 5 mM Ca^{2+} are colored dark-gray (12, 22, 24, 40, 69, 83, 89–94, 96, 99–100, 102–104 and 106–107). Selected residue numbers are indicated as references.

NMR spectra indicate that high-affinity calcium binding results in a major conformational change (Figure 6A). Residues least affected by calcium binding reside mostly within the C-terminus of V6 (Figure 8E, colored dark-gray, residues 12, 22, 24, 40, 69, 83, 89–94, 96, 99, 100, 102–104, 106, and 107). Therefore, we expect the calcium-induced structural changes to occur in the first 80 residues of the polypeptide. The same part of V6 (residues 1–80) was indicated to be calcium-sensitive in the context of the V6-HP fragment.[7] The low-affinity calcium binding is associated with a more localized structural change at or near the long α-helix (Figure 6B). Of the five Trp residues in the V6 polypeptide, three reside in the calcium-insensitive C-terminal region (Figure 8A). Therefore, the calcium-induced changes in the fluorescence signal are mostly due to the centrally located Trp37 and Trp43. The NMR chemical shift values of the side chain of Trp43, which we can reliably monitor across all the calcium levels tested, are sensitive to calcium (Figure 8D).

In calcium-bound V6, the long α-helix forms a hydrophobic contact with the adjacent residues of the central β-sheet (Figures 8A), strands A–D (Figure 4B). In both calcium-free and calcium-bound G6 (domain 6 of gelsolin), the long helix forms very similar hydrophobic contacts (Figure 8B,C). In the calcium-free G6 structure, Trp37 and Trp43 are exposed (Figure 8C). These residues become buried in the core of calcium-bound G6 (Figure 8B). By analogy, the tryptophan fluorescence quenching observed in V6 could be explained by the positioning of Trp37 and Trp43. We expect that the calcium-induced changes in V6 cause Trp37 and Trp43 to become less exposed as in G6 (Figure 8B), resulting in the observed fluorescence quenching (Figures 5 and 8A).

The low-affinity calcium binding also leads to conformational changes in the long α-helix and nearby residues in V6. The observed spectral changes of V6 in 5 and 1 mM Ca^{2+} (Figure 6B) allow us to identify positions sensitive to millimolar (K_d = 2.8 mM) levels of calcium. These residues (6, 10, 30–33, 45, 50, 52, 55, 57, 59, 62, 63, 65, 67, and 71) reside in the long α-helix and β-strands A–C (Figure 8E). Four of five residues (45, 52, 62, and 71), whose resonances are most significantly shifted between spectra at 5 and 1 mM Ca^{2+}, are also positioned at or near the long helix. The long helix contains four clustered acidic residues (Glu50, Glu54, Glu58, and Glu62) that form a contiguous, solvent-exposed side chain ridge. This likely explains the sensitivity of the helix to millimolar calcium levels.

Our tryptophan fluorescence and NMR data are consistent in identifying both calcium binding regimes in V6 (micromolar and millimolar). Furthermore, the micromolar affinity of V6 for calcium derived from our data is lower than that reported for the calcium binding of G5 and G6 (K_d = 0.2 μM)[55] and higher than that of villin domain 1 (also known as 14T[56,57]), which is in the millimolar range. The micromolar affinity of V6 for calcium suggests its role in activation of the F-actin severing function in intact villin triggered by increased intracellular calcium levels (200 μM).[2] Our combined data agree with the straightening of the long helix in V6 upon calcium binding (as in G6)[8,9] and the "latch and hinge" mechanism. Villin is known to undergo a major conformational change induced by ~20 μM calcium.[21] The long helix-containing core of V6 also undergoes substantial conformational changes at the same calcium level (K_d of 22 μM). Therefore, we propose that V6 acts as a calcium-activated trigger for these major alterations in intact villin. The physiological relevance of the millimolar Ca^{2+}

dx.doi.org/10.1021/bi400699s | Biochemistry 2013, 52, 7890–7900

binding to V6 is unclear and likely minor, because the related conformational changes are small (Figure 6B).

In the recent crystal structure of a calcium-free human villin construct containing domains V4−V6 in the presence of actin, the V6 domain long helix is straight,[24] in contrast to the kinked long helix observed for calcium-free G6.[9] The extent to which villin domains 4 and 5 (V4 and V5, respectively), which are not visible in the structure, influence the geometry of the long helix conformation of V6 in the crystal is, however, unclear.[24] Our present V6 solution structure shows that the main helix is straight at high calcium concentrations (Figure 4), consistent with the calcium-bound state of G6[25] (Figure 8A,B). Our calcium back-titration indicates that the V6 long helix undergoes a conformational change upon calcium binding (Figure 6), likely to a G6-style kinked conformation (Figure 8C).[9] The conformational switch associated with the long helix area in V6 may play a fundamental role in controlling the many functions of villin. We are currently working on the solution structure of the calcium-free V6 domain to clarify whether the long helix of V6 is straight or kinked in the absence of calcium.

V6 Is Monomeric and Cannot Bind F-Actin, Implicating the V6-to-HP Linker in F-Actin Binding. At 5 mM calcium, the V6 domain adopts the same fold in isolation and in V6-HP (Figure 3). This suggests that isolated V6 and V6-HP have the same calcium-sensitive areas because the HP domain is insensitive to calcium.[14,22,23] Both V6 (Figure 2) and V6-HP[7] are monomeric at high calcium concentrations. To determine whether isolated V6 contains a suggested cryptic F-actin binding site[7] and can bind F-actin, we performed a sedimentation assay (Figure 7). The isolated V6 cannot bind F-actin regardless of the level of calcium. One of the most likely explanations here is that V6-HP utilizes a part of the disordered, 40-residue interdomain linker in V6-HP along with V6 to form the second, cryptic F-actin binding site. The short α-helix at the C-terminus of V6 (positions 98−102) is not bound tightly to the core of the domain and may form the beginning of the V6-to-HP linker fragment implicated in the formation of an actin binding site. The structural features of the linker may change upon alterations in calcium levels or actin binding.

Our gel filtration data show that isolated V6 remains monomeric at any calcium level tested (Figure 2), whereas V6-HP aggregates[7] at low calcium levels. This implicates the disordered V6-to-HP linker as a necessary part of V6-HP aggregation as the isolated HP is a calcium-insensitive monomer.[14,22,23] Work is currently in progress in our lab to test the role of the V6-to-HP linker in actin binding and V6-HP aggregation.

CONCLUSION

In our tests, V6 remains monomeric and does not bind actin filaments (with or without calcium). The role of the V6-to-HP linker in F-actin binding and oligomerization is currently under investigation in our lab. We show that the isolated V6 domain of villin adopts a typical gelsolin-like fold at high calcium concentrations. On the basis of our solution NMR data, the calcium-bound domain adopts a nearly identical fold in isolation and in the V6-HP fragment. At high calcium concentrations, the long helix in V6 adopts the extended conformation. The long α-helix and β-sheet core form the most calcium-sensitive part of the V6 domain, like G6 in gelsolin. We suggest that the long helix in calcium-free V6 adopts a kinked conformation in accordance with the "latch and hinge" activation mechanism. Overall, the affinity of V6 for calcium and the corresponding conformational changes in the domain and intact protein at 20 μM Ca^{2+} implicate V6 as the switch for the F-actin severing function in villin (threshold of 200 μM Ca^{2+}). The exact conformation of the long helix in calcium-free V6 and the location of the calcium sites are under investigation in our lab. Such an investigation will result in a clearer understanding of calcium regulation of V6 and provide needed insight into activation of the many functions of the modular F-actin regulator villin.

ASSOCIATED CONTENT

Supporting Information

Supplementary figures describing additional NMR data, fitting of the intrinsic tryptophan fluorescence under the one-K_d and two-K_d models, and SDS−PAGE purity analysis of V6. This material is available free of charge via the Internet at http://pubs.acs.org.

Accession Codes

The ^{1}H, ^{15}N, and ^{13}C NMR assignments for the V6 sample reported here have been deposited in the Biological Magnetic Resonance Bank as entry 18046. The atomic-resolution solution structure of the V6 protein sample reported here has been deposited in the Protein Data Bank as entry 2LLF.

AUTHOR INFORMATION

Corresponding Author

*E-mail: smirnov@chem.wwu.edu. Telephone: (360) 650-2302. Fax: (360) 650-2826.

Author Contributions

S.O.F., J.B., and D.A.P. contributed equally to this work.

Funding

This work was supported by the Murdock Charitable Trust and startup funding from Western Washington University to S.L.S.

Notes

The authors declare no competing financial interest.

ACKNOWLEDGMENTS

We are grateful to David Gruber, Heather Miears, and Joanna Hoppins (Western Washington University) for their help with preparation of the manuscript. A portion of the work was performed at the National High Magnetic Field Laboratory, which is supported by National Science Foundation Cooperative Agreement DMR-0654118, the State of Florida, and the U.S. Department of Energy. Part of the work was conducted using scientific equipment of the Center of Shared Usage "The analytical center of nano- and biotechnologies of SPbSPU" with financial support of the Ministry of Education and Science of the Russian Federation (Agreement 14.B37.21.1230).

ABBREVIATIONS

DTT, dithiothreitol; F-actin, filamentous actin; G-actin, globular actin; IPTG, isopropyl β-D-1-thiogalactopyranoside; EDTA, ethylenediaminetetraacetic acid; NOE, nuclear Overhauser effect; PIP2, phosphatidylinositol 4,5-bisphosphate; PIPES, piperazine-1,4-bis(2-ethanesulfonic acid); NMR, nuclear magnetic resonance; OD, optical density; MWCO, molecular weight cutoff; SEC, size-exclusion chromatography.

REFERENCES

(1) Khurana, S., and George, S. P. (2008) Regulation of cell structure and function by actin-binding proteins: Villin's perspective. *FEBS Lett. 582*, 2128−2139.

(2) Bretscher, A., and Weber, K. (1980) Villin is a major protein of the microvillus cytoskeleton which binds both G and F actin in a calcium-dependent manner. *Cell 20*, 839−847.

(3) Andre, E., Lottspeich, F., Schleicher, M., and Noegel, A. (1988) Severin, gelsolin, and villin share a homologous sequence in regions presumed to contain F-actin severing domains. *J. Biol. Chem. 263*, 722−727.

(4) Pestonjamasp, K. N., Pope, R. K., Wulfkuhle, J. D., and Luna, E. J. (1997) Supervillin (p205): A novel membrane-associated, F-actin-binding protein in the villin/gelsolin superfamily. *J. Cell Biol. 139*, 1255−1269.

(5) Gangopadhyay, S. S., Takizawa, N., Gallant, C., Barber, A. L., Je, H. D., Smith, T. C., Luna, E. J., and Morgan, K. G. (2004) Smooth muscle archvillin: A novel regulator of signaling and contractility in vascular smooth muscle. *J. Cell Sci. 117*, 5043−5057.

(6) Oh, S. W., Pope, R. K., Smith, K. P., Crowley, J. L., Nebl, T., Lawrence, J. B., and Luna, E. J. (2003) Archvillin, a muscle-specific isoform of supervillin, is an early expressed component of the costameric membrane skeleton. *J. Cell Sci. 116*, 2261−2275.

(7) Smirnov, S. L., Isern, N. G., Jiang, Z. G., Hoyt, D. W., and McKnight, C. J. (2007) The Isolated Sixth Gelsolin Repeat and Headpiece Domain of Villin Bundle F-Actin in the Presence of Calcium and Are Linked by a 40-Residue Unstructured Sequence. *Biochemistry 46*, 7488−7496.

(8) Kolappan, S., Gooch, J. T., Weeds, A. G., and McLaughlin, P. J. (2003) Gelsolin domains 4−6 in active, actin-free conformation identifies sites of regulatory calcium ions. *J. Mol. Biol. 329*, 85−92.

(9) Burtnick, L. D., Koepf, E. K., Grimes, J., Jones, E. Y., Stuart, D. I., McLaughlin, P. J., and Robinson, R. C. (1997) The crystal structure of plasma gelsolin: Implications for actin severing, capping, and nucleation. *Cell 90*, 661−670.

(10) Kumar, N., Zhao, P., Tomar, A., Galea, C. A., and Khurana, S. (2004) Association of villin with phosphatidylinositol 4,5-bisphosphate regulates the actin cytoskeleton. *J. Biol. Chem. 279*, 3096−3110.

(11) Kumar, N., and Khurana, S. (2004) Identification of a functional switch for actin severing by cytoskeletal proteins. *J. Biol. Chem. 279*, 24915−24918.

(12) Friederich, E., Vancompernolle, K., Louvard, D., and Vandekerckhove, J. (1999) Villin function in the organization of the actin cytoskeleton. Correlation of in vivo effects to its biochemical activities in vitro. *J. Biol. Chem. 274*, 26751−26760.

(13) Ferrary, E., Cohen-Tannoudji, M., Pehau-Arnaudet, G., Lapillonne, A., Athman, R., Ruiz, T., Boulouha, L., El Marjou, F., Doye, A., Fontaine, J. J., Antony, C., Babinet, C., Louvard, D., Jaisser, F., and Robine, S. (1999) In vivo, villin is required for Ca^{2+}-dependent F-actin disruption in intestinal brush borders. *J. Cell Biol. 146*, 819−830.

(14) Finidori, J., Friederich, E., Kwiatkowski, D. J., and Louvard, D. (1992) In vivo analysis of functional domains from villin and gelsolin. *J. Cell Biol. 116*, 1145−1155.

(15) Pope, B., Way, M., Matsudaira, P. T., and Weeds, A. (1994) Characterisation of the F-actin binding domains of villin: Classification of F-actin binding proteins into two groups according to their binding sites on actin. *FEBS Lett. 338*, 58−62.

(16) George, S. P., Wang, Y., Mathew, S., Srinivasan, K., and Khurana, S. (2007) Dimerization and actin-bundling properties of villin and its role in the assembly of epithelial cell brush borders. *J. Biol. Chem. 282*, 26528−26541.

(17) Hampton, C. M., Liu, J., Taylor, D. W., DeRosier, D. J., and Taylor, K. A. (2008) The 3D structure of villin as an unusual F-actin crosslinker. *Structure 16*, 1882−1891.

(18) McGough, A. M., Staiger, C. J., Min, J. K., and Simonetti, K. D. (2003) The gelsolin family of actin regulatory proteins: Modular structures, versatile functions. *FEBS Lett. 552*, 75−81.

(19) Walsh, T. P., Weber, A., Davis, K., Bonder, E., and Mooseker, M. (1984) Calcium dependence of villin-induced actin depolymerization. *Biochemistry 23*, 6099−6102.

(20) Silacci, P., Mazzolai, L., Gauci, C., Stergiopulos, N., Yin, H. L., and Hayoz, D. (2004) Gelsolin superfamily proteins: Key regulators of cellular functions. *Cell. Mol. Life Sci. 61*, 2614−2623.

(21) Hesterberg, L. K., and Weber, K. (1983) Ligand-induced conformational changes in villin, a calcium-controlled actin-modulating protein. *J. Biol. Chem. 258*, 359−364.

(22) Meng, J., Vardar, D., Wang, Y., Guo, H. C., Head, J. F., and McKnight, C. J. (2005) High-resolution crystal structures of villin headpiece and mutants with reduced F-actin binding activity. *Biochemistry 44*, 11963−11973.

(23) Vardar, D., Buckley, D. A., Frank, B. S., and McKnight, C. J. (1999) NMR structure of an F-actin-binding "headpiece" motif from villin. *J. Mol. Biol. 294*, 1299−1310.

(24) Wang, H., Chumnarnsilpa, S., Loonchanta, A., Li, Q., Kuan, Y. M., Robine, S., Larsson, M., Mihalek, I., Burtnick, L. D., and Robinson, R. C. (2009) Helix straightening as an activation mechanism in the gelsolin superfamily of actin regulatory proteins. *J. Biol. Chem. 284*, 21265−21269.

(25) Choe, H., Burtnick, L. D., Mejillano, M., Yin, H. L., Robinson, R. C., and Choe, S. (2002) The calcium activation of gelsolin: Insights from the 3 Å structure of the G4-G6/actin complex. *J. Mol. Biol. 324*, 691−702.

(26) Marley, J., Lu, M., and Bracken, C. (2001) A method for efficient isotopic labeling of recombinant proteins. *J. Biomol. NMR 20*, 71−75.

(27) Edelhoch, H. (1967) Spectroscopic determination of tryptophan and tyrosine in proteins. *Biochemistry 6*, 1948−1954.

(28) Delaglio, F., Grzesiek, S., Vuister, G. W., Zhu, G., Pfeifer, J., and Bax, A. (1995) NMRPipe: A multidimensional spectral processing system based on UNIX pipes. *J. Biomol. NMR 6*, 277−293.

(29) Kay, L. E., Keifer, P., and Saarinen, T. (1992) Pure absorption gradient enhanced heteronuclear single quantum correlation spectroscopy with improved sensitivity. *J. Am. Chem. Soc. 114*, 10663−10665.

(30) Palmer, A. G., Cavanagh, J., Wright, P. E., and Rance, M. (1991) Sensitivity improvement in proton-detected two-dimensional heteronuclear correlation NMR spectroscopy. *J. Magn. Reson. 93*, 151−170.

(31) Muhandiram, D. R., and Kay, L. E. (1994) Gradient-Enhanced Triple-Resonance Three-Dimensional NMR Experiments with Improved Sensitivity. *J. Magn. Reson., Ser. B 103*, 203−216.

(32) Wittekind, M., and Mueller, L. (1993) HNCACB, a High-Sensitivity 3D NMR Experiment to Correlate Amide-Proton and Nitrogen Resonances with the α- and β-Carbon Resonances in Proteins. *J. Magn. Reson., Ser. B 101*, 201−205.

(33) Grzesiek, S., and Bax, A. (1992) Correlating backbone amide and side chain resonances in larger proteins by multiple relayed triple resonance NMR. *J. Am. Chem. Soc. 114*, 6291−6293.

(34) Grzesiek, S., and Bax, A. (1992) Improved 3D triple-resonance NMR techniques applied to a 31 kDa protein. *J. Magn. Reson. 96*, 432−440.

(35) Yamazaki, T., Lee, W., Arrowsmith, C. H., Muhandiram, D. R., and Kay, L. E. (1994) A Suite of Triple Resonance NMR Experiments for the Backbone Assignment of ^{15}N, ^{13}C, ^{2}H Labeled Proteins with High Sensitivity. *J. Am. Chem. Soc. 116* (26), 11655−11666.

(36) Vuister, G. W., and Bax, A. (1993) Quantitative J correlation: A new approach for measuring homonuclear three-bond $J_{HNH\alpha}$ coupling constants in ^{15}N-enriched proteins. *J. Am. Chem. Soc. 115* (17), 7772−7777.

(37) Archer, S. J., Ikura, M., Torchia, D. A., and Bax, A. (1991) An alternative 3D NMR technique for correlating backbone ^{15}N with side chain Hβ resonances in larger proteins. *J. Magn. Reson. 95*, 636−641.

(38) Grzesiek, S., and Bax, A. (1993) Amino acid type determination in the sequential assignment procedure of uniformly $^{13}C/^{15}N$-enriched proteins. *J. Biomol. NMR. 3*, 185−204.

(39) Bahrami, A., Assadi, A. H., Markley, J. L., and Eghbalnia, H. R. (2009) Probabilistic interaction network of evidence algorithm and its

application to complete labeling of peak lists from protein NMR spectroscopy. *PLoS Comput. Biol. 5*, e1000307.
(40) Clore, G. M., Bax, A., Driscoll, P. C., Wingfield, P. T., and Gronenborn, A. M. (1990) Assignment of the side-chain ^{1}H and ^{13}C resonances of interleukin-1β using double- and triple-resonance heteronuclear three-dimensional NMR spectroscopy. *Biochemistry 29* (35), 8172−8184.
(41) Bax, A., Clore, G. M., and Gronenborn, A. M. (1990) ^{1}H-^{1}H correlation via isotropic mixing of ^{13}C magnetization, a new three-dimensional approach for assigning ^{1}H and ^{13}C spectra of ^{13}C-enriched proteins. *J. Magn. Reson. 88*, 425−431.
(42) Grzesiek, S., Anglister, J., and Bax, A. (1993) Correlation of Backbone Amide and Aliphatic Side-Chain Resonances in $^{13}C/^{15}N$-Enriched Proteins by Isotropic Mixing of ^{13}C Magnetization. *J. Magn. Reson., Ser. B 101*, 114−119.
(43) States, D. J., Haberkorn, R. A., and Ruben, D. J. (1982) A two-dimensional nuclear overhauser experiment with pure absorption phase in four quadrants. *J. Magn. Reson. 48*, 286−292.
(44) Johnson, B. A., and Blevins, R. A. (1994) NMRView: A computer program for the visualization and analysis of NMR data. *J. Biomol. NMR 4*, 603−614.
(45) Wishart, D. S., Bigam, C. G., Yao, J., Abildgaard, F., Dyson, H. J., Oldfield, E., Markley, J. L., and Sykes, B. D. (1995) ^{1}H, ^{13}C and ^{15}N chemical shift referencing in biomolecular NMR. *J. Biomol. NMR 6*, 135−140.
(46) Guntert, P. (2004) Automated NMR structure calculation with CYANA. *Methods Mol. Biol. 278*, 353−378.
(47) Berjanskii, M. V., Neal, S., and Wishart, D. S. (2006) PREDITOR: A web server for predicting protein torsion angle restraints. *Nucleic Acids Res. 34*, W63−W69.
(48) Sayle, R. A., and Milner-White, E. J. (1995) RASMOL: Biomolecular graphics for all. *Trends Biochem. Sci. 20*, 374.
(49) Pettersen, E. F., Goddard, T. D., Huang, C. C., Couch, G. S., Greenblatt, D. M., Meng, E. C., and Ferrin, T. E. (2004) UCSF Chimera: A visualization system for exploratory research and analysis. *J. Comput. Chem. 25*, 1605−1612.
(50) Bhattacharya, A., Tejero, R., and Montelione, G. T. (2007) Evaluating protein structures determined by structural genomics consortia. *Proteins 66*, 778−795.
(51) Kumar, N., Tomar, A., Parrill, A. L., and Khurana, S. (2004) Functional dissection and molecular characterization of calcium-sensitive actin-capping and actin-depolymerizing sites in villin. *J. Biol. Chem. 279*, 45036−45046.
(52) Motulsky, H. (1996) *The GraphPad Guide to Analyzing Radioligand Binding Data*, e-book, GraphPad Software, Inc., La Jolla, CA.
(53) Prager, E. M., and Jolles, P. (1996) Animal lysozymes c and g: An overview. *EXS 75*, 9−31.
(54) Lomax, R. G., and Hahs-Vaughn, D. L. (2007) *Statistical Concepts: A Second Course*, 3rd ed., Taylor & Francis, New York.
(55) Robinson, R. C., Mejillano, M., Le, V. P., Burtnick, L. D., Yin, H. L., and Choe, S. (1999) Domain movement in gelsolin: A calcium-activated switch. *Science 286*, 1939−1942.
(56) Markus, M. A., Matsudaira, P., and Wagner, G. (1997) Refined structure of villin 14T and a detailed comparison with other actin-severing domains. *Protein Sci. 6*, 1197−1209.
(57) Markus, M. A., Nakayama, T., Matsudaira, P., and Wagner, G. (1994) Solution structure of villin 14T, a domain conserved among actin-severing proteins. *Protein Sci. 3*, 70−81.
(58) Larkin, M. A., Blackshields, G., Brown, N. P., Chenna, R., McGettigan, P. A., McWilliam, H., Valentin, F., Wallace, I. M., Wilm, A., Lopez, R., Thompson, J. D., Gibson, T. J., and Higgins, D. G. (2007) Clustal W and Clustal X version 2.0. *Bioinformatics 23*, 2947−2948.